

# Journal of Materials Chemistry A

Accepted Manuscript



This article can be cited before page numbers have been issued, to do this please use: H. Banda, D. Damien, K. Nagarajan, M. Hariharan and M. M. Shaijumon, *J. Mater. Chem. A*, 2015, DOI: 10.1039/C5TA02043C.



This is an *Accepted Manuscript*, which has been through the Royal Society of Chemistry peer review process and has been accepted for publication.

*Accepted Manuscripts* are published online shortly after acceptance, before technical editing, formatting and proof reading. Using this free service, authors can make their results available to the community, in citable form, before we publish the edited article. We will replace this *Accepted Manuscript* with the edited and formatted *Advance Article* as soon as it is available.

You can find more information about *Accepted Manuscripts* in the [Information for Authors](#).

Please note that technical editing may introduce minor changes to the text and/or graphics, which may alter content. The journal's standard [Terms & Conditions](#) and the [Ethical guidelines](#) still apply. In no event shall the Royal Society of Chemistry be held responsible for any errors or omissions in this *Accepted Manuscript* or any consequences arising from the use of any information it contains.

## ARTICLE

## Polyimide based all-organic sodium ion battery

Cite this: DOI: 10.1039/x0xx00000x

Harish Banda,<sup>a,b</sup> Dijo Damien,<sup>a,b</sup> Kalaivanan Nagarajan,<sup>b</sup> Mahesh Hariharan<sup>b</sup> and Manikoth M. Shaijumon<sup>a\*</sup>Received 00th January 2012,  
Accepted 00th January 2012

DOI: 10.1039/x0xx00000x

www.rsc.org/

Developing new approaches to improve the performance of organic electrodes for rechargeable sodium batteries is important. Here we report studies on N,N'-diamino-3,4,9,10-pyrenetetracarboxylic polyimide (PI) as a novel cathode for sodium battery and demonstrate an all-organic sodium ion battery using this polyimide as cathode and disodium terephthalate (NaTP) (pre-sodiated) as anode. The synthesised PI exhibits excellent electrochemical properties, when studied as cathode for sodium batteries, with a reversible capacity of 126 mAhg<sup>-1</sup> along with good capacity retention and rate capability, in the voltage range of 1.5 to 3.5 V vs. Na<sup>+</sup>/Na. The all-organic sodium ion full cell delivered an initial capacity of 73 mAhg<sup>-1</sup>, with an average cell voltage of 1.35 V. The attractive electrochemical performance combined with the design flexibility of PTCDA based PI material, offer new possibilities for the development of efficient all-organic sodium batteries.

## 1. Introduction

Lithium ion batteries (LIBs) have been at the forefront of energy storage technologies for a range of portable device applications over the past couple of decades and have been recently looked at to meet the on-board energy requirements in vehicular applications. However, with the recent concerns on the availability of lithium and the high cost associated with bulk production of LIBs, sodium ion batteries (SIBs) have been regarded as a promising alternative to LIBs, particularly for large-scale applications.<sup>1-3</sup> Recently, there has been great interest in developing advanced electrode materials for SIBs, and a large number of materials involving transition metals have been proposed as cathodes, similar to those explored for LIBs.<sup>4-8</sup> While high voltage and good cyclability have been the thriving factors for these materials, the associated environmental concerns and their higher production costs question the long term reliance on these inorganic materials used in SIBs for large-scale applications. Organic materials, owing to their abundance, design flexibility and environmental benignancy, have lately enjoyed a renewed interest as electrodes in rechargeable lithium batteries.<sup>9-11</sup> Various reports demonstrating high lithium storage capacities, possible multi-electron reactions and tuneable redox potentials have appeared recently in the literature.<sup>12-20</sup> The mechanism of lithiation/de-lithiation in organic compounds involves reversible redox reaction of the respective organic functional groups such as keto, carboxylate, anhydride, and so on along with

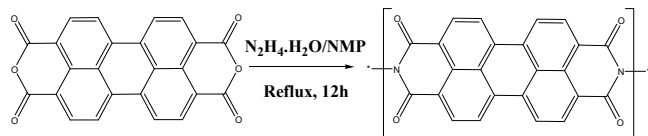
insertion/removal of Li<sup>+</sup> ions at the respective redox centres. The enolates thus formed are stabilized by extended conjugation in the aromatic rings.

One of the key challenges for organic electrode materials is the dissolution of active material into electrolytes during charge-discharge cycling, resulting in poor cycling performances.<sup>21, 22</sup> Several strategies have been suggested to resolve the dissolution issue, such as non-covalent or covalent attachment of redox molecules to substrates, polymerization of active compound, optimization of molecular structure, and the use of solid electrolytes.<sup>21, 23-28</sup> Polymerisation of active compound is particularly interesting owing to its versatility and the added advantages of improved thermal stability and increased kinetics of electron transfer through polymer chains.<sup>21, 23</sup>

Unfortunately, the progress on organic electrode materials on the sodium front has been limited and only very recently, the work on organic based electrodes for SIBs did gain momentum.<sup>29-34</sup> Polyimides, with their good thermal stability and electronic conductivity,<sup>24</sup> undergo reversible sodiation/de-sodiation processes alongside the redox conversion of imide functionality to enolate. Recent reports on 1,4,5,8-naphthalenetetracarboxylic dianhydride (NTCDA) derived polyimides as cathodes for SIBs show good cycling stability and power capability but offer lower voltages.<sup>35, 36</sup> 3,4,9,10-perylenetetracarboxylic dianhydride (PTCDA) derived polyimides offer higher reduction potentials and in turn higher energy densities.<sup>37</sup> Zhang *et al.* demonstrated various diamines as polymerising agents for PTCDA.<sup>38</sup> Ethylene diamine, 1,3-

propylene diamine and other long chain diamines used, offer an inherent electrochemical dead weight and lead to lower gravimetric specific capacities. Further, Abouimrane *et al.* demonstrated a sodium ion full cell incorporating a disodium terephthalate based organic anode material with traditional transition metal oxide based materials as cathode.<sup>39</sup> NTCDA derived polyimides based sodium ion full cells have also been demonstrated, but with conventional inorganic materials as cathodes.<sup>35, 36</sup> All organic sodium ion full cells with p-doped polymer and organic salt based electrodes have recently been reported respectively by Yang *et al.*<sup>40</sup> and Wang *et al.*<sup>32</sup> Previously, we reported various polyimides derived from 3,4,9,10-perylene-tetracarboxylic dianhydride (PTCDA) as electrodes for LIBs with higher reduction potentials and good rate capabilities.<sup>23</sup>

Herein, we report the studies on N,N'-diamino-3,4,9,10-perylene-tetracarboxylic polyimide (PI), based on PTCDA, as a novel cathode material for rechargeable SIBs. The material has been prepared following similar chemistry as in our previous report,<sup>23</sup> with slight modification to the synthesis protocol. The synthesised PI, with a theoretical capacity of 257 mAhg<sup>-1</sup> corresponding to a four electron redox process, exhibits good electrochemical activity in the voltage range of 1.5 to 3.5 V vs. Na<sup>+</sup>/Na, with a reversible capacity of 126 mAhg<sup>-1</sup>, and with good rate capability. Further, an all-organic sodium ion full cell based on polyimides is demonstrated for the first time, using disodium terephthalate (NaTP) as anode material and the synthesised PI as cathode. The full cell exhibits an average discharge voltage of 1.35 V.



**Scheme 1:** Schematic diagram for the synthesis of PI.

## 2. Experimental Section

### 2.1 Materials synthesis

PI was synthesized by modifying a protocol (Scheme 1) we reported elsewhere.<sup>23</sup> Equimolar PTCDA (1 g, 2.55 mmol) and hydrazine monohydrate (127.5 mg, 2.55 mmol) reacted under reflux conditions in N-methyl-2-pyrrolidone solvent (50 ml) for 6 h under an inert atmosphere. The residue was filtered, washed with ethanol and dried at 120 °C in vacuum for 12 h. N,N'-diamino-3,4,9,10-perylene-tetracarboxylic polyimide is also synthesised in imidazole medium as reported earlier and this will be referred as PI-IMI here after. Briefly, a mixture of 2 mmol of 3,4,9,10-perylene-tetracarboxylic dianhydride (PTCDA), 2 mmol of diamine, 5.0 g of imidazole and 2 mmol of zinc acetate was heated with stirring at 140 °C for 5 h. The mixture was cooled and poured into 1 N hydrochloric acid. Precipitate was collected through vacuum filtration and washed with boiling saturated potassium carbonate solution followed by distilled water. The product is dried in air at 100 °C. Model

derivative PTCDA was used as such purchased from Sigma Aldrich. The molten state synthesis technique with imidazole as the solvent involves extensive washing procedures and also result in particles of several microns of size. A solution based synthesis with N-methyl-2-pyrrolidone was thus preferred to this molten state synthesis technique.

The NaTP was synthesized following a recrystallization method reported by Park *et al.*<sup>29</sup> Briefly, Terephthalic acid (1.5 g, 9.04 mmol) was added to solution of sodium hydroxide (0.91 g, 22.6 mmol) in deionized water (DI water, 5 ml) at 60 °C. DI water was gradually added to the solution at 90 °C until the solution started to show precipitation. After refluxing at 90 °C for 12 h, the crystal was hot-filtered and then dried in vacuum at 120 °C for 2 h.

### 2.2 Materials characterization

Fourier transform infrared spectra were recorded on a Shimadzu IR Prestige-21 FT-IR spectrometer with KBr pellets. CHNS analysis was carried out on an Elementary vario MICRO cube elemental analyser. Powder X-ray diffraction (XRD) patterns were obtained using Empyrean, PANalytical instrument with reference radiation of Cu K $\alpha$  = 1.540 Å in the range 5-80°. Solid-state <sup>13</sup>C MAS NMR measurement was performed on a Bruker Avance 400 (400 MHz) spectrometer with a MAS rate of 5 kHz. <sup>1</sup>H NMR measurement was performed on Bruker Avance 500 (500 MHz) spectrometer. Scanning electron microscopy (SEM) images were recorded on a Nova NanoSEM450 FEI scanning electron microscope working at variable voltages from 10 to 30 kV. Thermo gravimetric analysis (TGA) was performed using a SDT Q600 Thermo gravimetric analyser (TA Instruments). All the electrochemical characterization was carried out using Biologic SAS VMP3 electrochemical workstation. Porosity characteristics of the samples were studied using N<sub>2</sub> adsorption-desorption isotherms measured at 77 K up to a maximum relative pressure of 1 bar, with the Micrometrics 3-Flex surface characterization analyser.

### 2.3 Electrochemical measurements

The PI based electrodes were fabricated by mixing active material, acetylene black and polyvinylidene fluoride (PVDF) in N-methyl-2-pyrrolidone (NMP) at a weight ratio of 60:30:10. The slurry was casted uniformly on stainless steel discs and the electrodes were dried at 65 °C in air for 6 h prior to 12 h drying at 120 °C in vacuum. A similar procedure was adopted for NaTP electrodes with an active material, acetylene black and PVDF weight ratio of 50:37.5:12.5. Galvanostatic charge and discharge measurements on the fabricated electrodes were performed in a CR 2032 type coin cell assembled in an argon filled glove box with moisture and oxygen level maintained at less than 0.1 ppm. 1M NaPF<sub>6</sub> in propylene carbonate was used as the electrolyte in all the electrochemical measurements. Half-cell measurements were done using Na metal as reference and counter electrode. Full cell measurements were performed by using electrochemically sodiated NaTP as the anode and PI

as the cathode. The typical electrode mass loading of the active material is  $1.4 \text{ mg.cm}^{-2}$ .

### 3. Results and Discussion

#### 3.1 Structural and electrochemical characterization of PI

Fig. 1a shows broad FT-IR absorption peaks at  $1774 \text{ cm}^{-1}$  and  $1720 \text{ cm}^{-1}$  for PTCDA and two sharp peaks at around  $1701 \text{ cm}^{-1}$  and  $1662 \text{ cm}^{-1}$  for PI which correspond to the carbonyl ( $\text{C}=\text{O}$ ) asymmetric and stretching frequencies, respectively. The shifts in the carbonyl stretching frequencies suggest the conversion of anhydride functionality to imide functionality and the values match with previous report.<sup>23</sup> Phase purity of PI is confirmed from a comparison with the powder XRD patterns of PI-IMI reported earlier (Fig. 1b).<sup>23</sup> Though both patterns exhibit same  $2\theta$  values, it is interesting to look at the peak broadening in the case of PI compared to PI-IMI, which could be due to the reduced particle size as observed in the SEM image (Fig. 1c, d). The modified synthesis procedure results in the formation of PI nanorods of  $\sim 100 \text{ nm}$  diameter (Fig. 1c), while PI-IMI nanorods were of  $\sim 500 \text{ nm}$  in diameter (Fig. 1d). Formation of polyimides is further confirmed using solid state  $^{13}\text{C}$  MAS NMR spectra and CHNS elemental analysis (see characterization section, ESI). PI showed enhanced thermal stability compared to PTCDA as revealed from the TGA analysis (Fig. S1).<sup>41</sup>

Electrochemical performance of PI was studied by galvanostatic charge-discharge and cyclic voltammetry (CV) studies. CV was carried out to test the reversible ingress of sodium ion into the PI by scanning the potential between 1.5 and 3.5 V vs.  $\text{Na}^+/\text{Na}$  at a scan rate of  $0.02 \text{ mVs}^{-1}$  (Fig. 2a). A pair of reduction peaks at 2.45 and 1.86 V and a pair of oxidation peaks at 2.75 and 1.97 V was observed in the first cycle. The peaks are sharp and have similar intensities, areas and remain almost unchanged in the subsequent cycles. It is clear from the CV that both the oxidation and reduction processes have two continuous steps, which are possibly the

formation of the radical anion ( $\text{PI}^{\cdot-}$ ) and radical dianion ( $\text{PI}^{2\cdot-}$ ), respectively.<sup>42</sup> The peak positions in the CV are quite consistent with the galvanostatic charge-discharge voltage profiles (Fig. 2b) which showed voltage plateaus around 2.45 and 1.86 V in the discharge profile. The galvanostatic charge-discharge cycling was performed at a high current density of  $100 \text{ mA g}^{-1}$  in the voltage range of 1.5 to 3.5 V vs.  $\text{Na}^+/\text{Na}$ . An initial discharge capacity of  $126 \text{ mAh g}^{-1}$  was obtained and capacity retention of  $\sim 90\%$  was maintained after 50 cycles of galvanostatic charge-discharge (Fig. 2c). All the charge-discharge curves showed similar features with  $\sim 97\%$  coulombic efficiency throughout the cycling. The excellent capacity retention upon cycling is attributed to the insolubility of PI in the electrolyte and the high structural stability of the electrode. Hydrazine being the smallest possible diamine, contributes minimally to the electrochemical dead weight of the system in comparison with ethylene, propylene or other long chain diamines.<sup>38</sup> Thus, we observe higher specific capacities with PI. To study the rate capability of the electrode, charge-discharge cycling was performed at current densities ranging from 25 to  $800 \text{ mA g}^{-1}$  (Fig. 2d). A remarkable 75% capacity retention was observed at  $800 \text{ mA g}^{-1}$  compared to the specific discharge capacity at  $25 \text{ mA g}^{-1}$ . The polymerization of the PTCDA by hydrazine, as predicted, reduces dissolution of the active material into electrolyte and also results in improved kinetics of electron transfer, leading to better rate performances, as

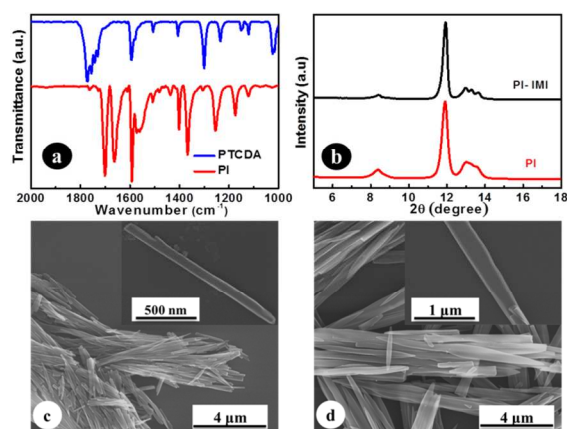


**Fig 1:** (a) FT-IR spectra for PTCDA and PI (KBr pellets), (b) Powder X-ray diffraction patterns for PI synthesised in N-methyl-2-pyrrolidone (PI) and in imidazole (PI-IMI), SEM micrographs of (c) PI and (d) PI-IMI, inset showing the respective high-resolution SEM images

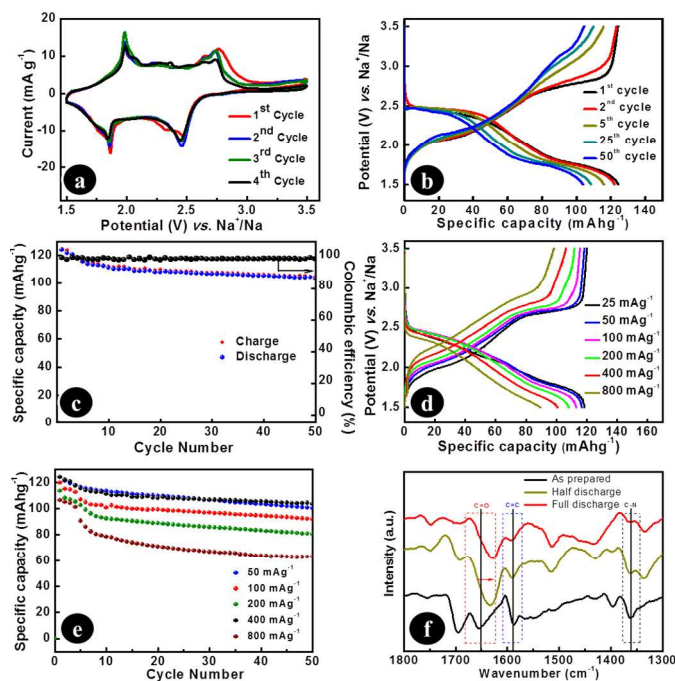
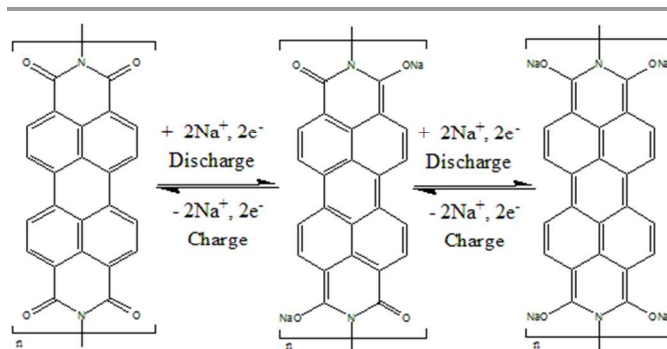


**Fig 2:** (a) Cyclic Voltammogram of PI scanned within 1.5 to 3.5 V vs.  $\text{Na}^+/\text{Na}$  at a scan rate  $0.02 \text{ mVs}^{-1}$  (b) Voltage profile of PI cycled at a current density of  $100 \text{ mA g}^{-1}$  in a voltage range of 1.5 to 3.5 V vs.  $\text{Na}^+/\text{Na}$  (c) Charge discharge cycling performance of PI galvanostatically cycled between 1.5 and 3.5 V vs.  $\text{Na}^+/\text{Na}$  at a current density of  $100 \text{ mA g}^{-1}$  (d) Charge-Discharge capacities of PI at different current densities. (e) Charge discharge cycling performance of PI galvanostatically cycled between 1.5 and 3.5 V vs.  $\text{Na}^+/\text{Na}$  at different current densities (f) FT-IR spectra for PI at different depths of discharge.



observed. Cycling stability at higher current densities of 50, 100, 200 and 400  $\text{mA g}^{-1}$  is also studied (Fig. 2e). A reversible specific discharge capacity of 80  $\text{mAh g}^{-1}$  was observed at high current density of 400  $\text{mA g}^{-1}$  after 50 cycles. With a high energy density of 181  $\text{Wh kg}^{-1}$  at a power density of 1,624  $\text{W kg}^{-1}$ , PI based electrodes exhibited excellent electrochemical properties, superior to recently reported polyimides and PTCDA based electrodes for SIBs.<sup>33, 35, 38</sup> A comparison of energy and power densities of PI with the reported polyimides is illustrated in the Ragone plot (Fig. S2). The chemical changes in the polyimide during the electrochemical events were investigated using FT-IR spectra (Fig. 2f). The spectra were taken for the fabricated electrodes at 3 different DOD viz., 0% (3.0V), 50% (2.25V) and 100% (1.5V) of the first cycle. The absorbance signals at 1590 and 1359  $\text{cm}^{-1}$  from the C=C stretching vibration in perylene ring and the C-N stretching vibration of imide, respectively, are unchanged, indicating that the carbon-carbon double bonds of the perylene core and carbon-nitrogen single bonds of the imide functionality remain intact during the electrochemical processes. Two sharp peaks at around 1698 and 1653  $\text{cm}^{-1}$ , which correspond to the carbonyl (C=O) asymmetric and stretching frequencies respectively are red shifted to a broad peak around 1630  $\text{cm}^{-1}$  during galvanostatic discharge. This corresponds to symmetric and asymmetric stretching of C-O-Na which in turn suggests the formation of enolate during discharge. Also, gradual reduction in the intensity of peak at 1696  $\text{cm}^{-1}$  suggests the conversion of imide functionality.<sup>38</sup> The obtained results are thus in accordance with the mechanism of reversible insertion/de-insertion of sodium ions through enolate formation (Scheme 2). The nanorod morphology with smaller dimensions offers reduced ion diffusion path lengths, which in turn result in good electrochemical performance even at higher current rates. This was further demonstrated by comparing the galvanostatic discharge profiles of PI and PI-IMI by discharging the electrodes at a slow rate of 10  $\text{mA g}^{-1}$ . PI showed a smoother and extended flat region with a discharge potential, 100 mV higher than PI-IMI (Fig. S3a). This can be attributed to the reduced ohmic resistance of the PI based electrodes. The modified synthesis route for polymerization facilitates the formation of this nanorod morphology with smaller dimensions. In addition,  $\text{N}_2$  adsorption-desorption isotherms and BET surface area analyses showed improved porosity characteristics for PI compared to PI-IMI (Fig. S3b). Though both the materials are meso-macro porous in nature, PI exhibits a BET surface area of 102  $\text{m}^2 \text{g}^{-1}$  compared to that of 41  $\text{m}^2 \text{g}^{-1}$  for PI-IMI. The enhanced cyclic stability of PI electrode compared to PI-IMI electrode (Fig. S3c) could be attributed to the structural stability of PI upon galvanostatic cycling. To further confirm this, an *ex-situ* SEM analysis of the fabricated PI electrodes before galvanostatic cycling (Fig. S4a) and after 50 cycles of galvanostatic cycling at a current density of 100  $\text{mA g}^{-1}$  (Fig. S4b) was performed. PI nanorods retain their nanorod morphology even after 50 cycles of galvanostatic charge and discharge. This reinforces the concept of polymerisation as an



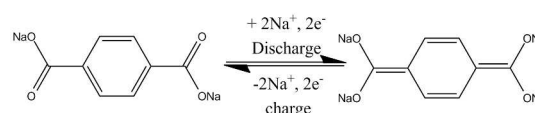
Scheme 2: Schematic representation of the charge-discharge mechanism in PI.

excellent strategy to prevent the electrode dissolution and to impart better mechanical properties for organic electrode materials. Encouraged by good electrochemical performance of PI, we chose to use this material as the cathode to fabricate an all-organic full cell.

### 3.2 Electrochemical characterization of PI-based all-organic full cell

An all-organic full cell is constructed using PI as the cathode material and disodium terephthalate (NaTP) as anode material. As-synthesized NaTP was well characterized using FT-IR, XRD and  $^1\text{H}$  NMR. An FT-IR spectrum for as-synthesised NaTP shows sharp peaks at 1551  $\text{cm}^{-1}$  and 1380  $\text{cm}^{-1}$ , which correspond to carboxylate asymmetric and symmetric stretching frequencies respectively (Fig. S5a). Also, the disappearance of broad peak around 3300–3600  $\text{cm}^{-1}$  corresponding to O-H stretching and the broad carbonyl stretching band at 1671  $\text{cm}^{-1}$  suggests the formation of salt. Formation of NaTP is confirmed using  $^1\text{H}$  NMR spectra (see characterization section, ESI). Further, thermo gravimetric analysis shows no weight loss in the sample around 320  $^\circ\text{C}$ , which suggests an absence of terephthalic acid monosodium salt (Fig. S5b). Phase purity of as-synthesised NaTP is confirmed using powder X-Ray diffraction technique and the pattern matches with ICDD reference number 00-052-2146 (Fig. S6).

Terephthalic acid disodium salt has previously been demonstrated as a promising anode material with a two sodium redox insertion process for sodium ion batteries (Scheme 3).<sup>29</sup> Fig. 3a shows the cyclic voltammogram for NaTP electrode scanned in the voltage range of 0 to 2 V at a scan rate of 0.02  $\text{mV s}^{-1}$  vs.  $\text{Na}^+/\text{Na}$ . Fig. 3b shows the galvanostatic charge-discharge voltage curve for NaTP cycled with a current density of 50  $\text{mA g}^{-1}$  in the voltage range of 0 to 2 V. A perfect coherence is observed between the redox peaks observed at 0.25 V at 0.05 V in the CV and voltage plateaus observed in the galvanostatic charge-discharge profiles.



Scheme 3: Schematic representation of charge-discharge mechanism for NaTP.

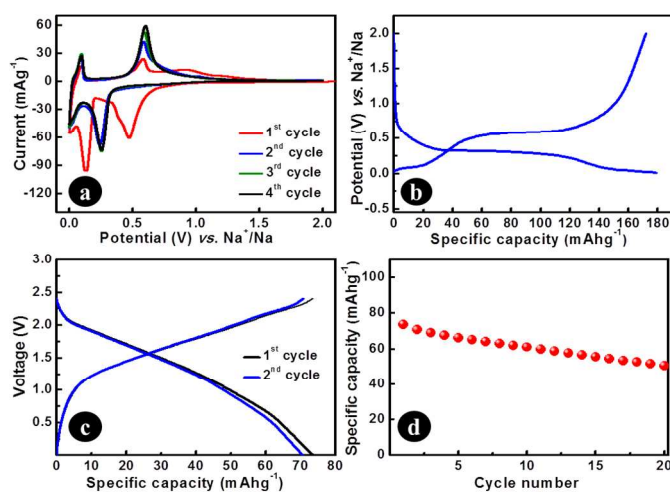


**Fig 3:** (a) Cyclic Voltammogram of NaTP scanned within 0 to 2 V vs.  $\text{Na}^+/\text{Na}$  at a scan rate  $0.02 \text{ mVs}^{-1}$  (b) Voltage profile of NaTP cycled at a current density of  $50 \text{ mA g}^{-1}$  in a voltage range of 0 to 2 V vs.  $\text{Na}^+/\text{Na}$ . (c) Voltage profile of PI-NaTP full-cell galvanostatically cycled at a current density of  $50 \text{ mA g}^{-1}$  in a voltage range of 0 to 2.4 V. (d) Cycling performance of PI-NaTP full-cell galvanostatically cycled at a current density of  $50 \text{ mA g}^{-1}$  in a voltage range of 0 to 2.4 V. Specific capacity is calculated based on the mass of both anode and active materials.

The peak at 0.25 V corresponds to the enolate formation of terephthalic carboxylate salt and the peak at 0.05 V corresponds to sodium ion insertion into conductive carbon additive.<sup>29</sup> A stable specific discharge capacity of around  $180 \text{ mAh g}^{-1}$  was obtained during the cycling. NaTP was thus chosen as the anode for the fabrication of an all-organic sodium ion full cell.

An all-organic sodium ion full cell using polyimide as cathode was realized for the first time by coupling it with electrochemically sodiated NaTP, as the anode. Electrochemical sodiation was done by discharging NaTP electrode to full capacity (0.1 V vs.  $\text{Na}^+/\text{Na}$ ) in a half cell configuration with a current density of  $50 \text{ mA g}^{-1}$ . Based on the stable specific discharge capacities obtained for the two electrodes, cathode and anode materials with optimized weight ratio of 1.6:1 was used to fabricate the full cell. The coin cells were galvanostatically cycled in the voltage window of 0 to 2.4 V at a current density of  $50 \text{ mA g}^{-1}$  (Fig 3c,d). The specific capacities of the full cell are calculated based on active material weights of both anode and cathode. The fabricated full cell exhibits an average discharge potential of 1.35 V with an initial specific capacity of  $73 \text{ mAh g}^{-1}$  (Fig. 3c), which is almost double the initial discharge capacity of  $40 \text{ mAh g}^{-1}$  observed for the full cell fabricated with NTCDA based polyimide as anode.<sup>36</sup> A gradual decrease in the specific capacity upon cycling was observed (Fig. 3d), which could be improved with further optimization of the electrode loading and other cell parameters.

## Conclusions

In summary, for the first time, we have demonstrated an all-organic sodium ion full cell using PTCDA based polyimide and disodium terephthalate (pre-sodiated) redox active molecules as cathode and anode respectively. As-synthesized PI exhibited

excellent electrochemical performance, when studied as cathode for rechargeable sodium battery, with a maximum energy density of  $254 \text{ Wh kg}^{-1}$  and a maximum power density of  $1,624 \text{ W kg}^{-1}$  when cycled against Na. While the half-cell measurements on PI electrode showed stable reversible capacity of  $126 \text{ mAh g}^{-1}$  with good capacity retention and rate capability, the all-organic sodium ion full cell delivered an initial capacity of  $73 \text{ mAh g}^{-1}$ . The excellent electrochemical performance of perylene polyimide material is attributed to the insolubility of the electrode in the electrolyte and its high structural stability. With the obtained attractive performances of PTCDA-based PI material, we believe that the present study will lead to new directions to tailor the organic materials for their applications in SIBs.

## Acknowledgements

H.B. acknowledges INSPIRE, Department of Science and Technology (DST), Govt. of India. D.D. and K.N acknowledge CSIR, Govt. of India, for the financial support. M.H. acknowledges the Science and Engineering Research Board, SERB/F/0962, for the partial financial support of this work. M.M.S. acknowledges Department of Biotechnology (DBT), Govt. of India, for financial support of this work through DBT's Twinning programme for the NE (BT/350/NE/TBP/2012).

## Notes and references

<sup>a</sup> School of Chemistry, Indian Institute of Science Education and Research Thiruvananthapuram, CET Campus, Sreekaryam, Thiruvananthapuram, Kerala, India. 695016.

<sup>b</sup> School of Physics, Indian Institute of Science Education and Research Thiruvananthapuram, CET Campus, Sreekaryam, Thiruvananthapuram, Kerala, India. 695016.

\* E-mail: shaiju@iisertvm.ac.in

† Electronic Supplementary Information (ESI) available: Characterization through FT-IR, XRD, TGA and electrochemical power capability studies. See DOI: 10.1039/c000000x/

1. S.-W. Kim, D.-H. Seo, X. Ma, G. Ceder and K. Kang, *Adv. Energy Mater.* 2012, **2**, 710.
2. H. Pan, Y.-S. Hu and L. Chen, *Energy Environ. Sci.* 2013, **6**, 2338.
3. V. Palomares, P. Serras, I. Villaluenga, K. B. Hueso, J. Carretero-Gonzalez and T. Rojo, *Energy Environ. Sci.* 2012, **5**, 5884.
4. Y. Cao, L. Xiao, W. Wang, D. Choi, Z. Nie, J. Yu, L. V. Saraf, Z. Yang and J. Liu, *Adv. Mater.* 2011, **23**, 3155.
5. N. Yabuuchi, M. Kajiyama, J. Iwatate, H. Nishikawa, S. Hitomi, R. Okuyama, R. Usui, Y. Yamada and S. Komaba, *Nat. Mater.* 2012, **11**, 512.
6. Z. Jian, W. Han, X. Lu, H. Yang, Y.-S. Hu, J. Zhou, Z. Zhou, J. Li, W. Chen, D. Chen and L. Chen, *Adv. Energy Mater.* 2013, **3**, 156.
7. C. S. Park, H. Kim, R. A. Shakoor, E. Yang, S. Y. Lim, R. Kahraman, Y. Jung and J. W. Choi, *J. Am. Chem. Soc.* 2013, **135**, 2787.
8. J. Qian, M. Zhou, Y. Cao, X. Ai and H. Yang, *Adv. Energy Mater.* 2012, **2**, 410.
9. M. Armand and J. M. Tarascon, *Nature* 2008, **451**, 652.

10. H. Chen, M. Armand, G. Demailly, F. Dolhem, P. Poizot and J.-M. Tarascon, *chemsuschem*. 2008, **1**, 348.
11. J.-M. Tarascon, *chemsuschem*. 2008, **1**, 777.
12. C. Luo, R. Huang, R. Kevorkyants, M. Pavanello, H. He and C. Wang, *Nano Letters* 2014, **14**, 1596.
13. Y. Morita, S. Nishida, T. Murata, M. Moriguchi, A. Ueda, M. Satoh, K. Arifuku, K. Sato and T. Takui, *Nat. Mater.* 2011, **10**, 947.
14. Y. Liang, P. Zhang and J. Chen, *Chem. Sci.* 2013, **4**, 1330.
15. H. Chen, M. Armand, M. Courty, M. Jiang, C. P. Grey, F. Dolhem, J.-M. Tarascon and P. Poizot, *J. Am. Chem. Soc.* 2009, **131**, 8984.
16. K. Sakaushi, G. Nickerl, F. M. Wieser, D. Nishio-Hamane, E. Hosono, H. Zhou, S. Kaskel and J. Eckert, *Angew. Chem., Int. Ed.* 2012, **51**, 7850.
17. Z. Song, H. Zhan and Y. Zhou, *Angew. Chem., Int. Ed.* 2010, **49**, 8444.
18. Y. Liang, P. Zhang, S. Yang, Z. Tao and J. Chen, *Adv. Energy Mater.* 2013, **3**, 600.
19. M. Armand, S. Grugeon, H. Vezin, S. Laruelle, P. Ribiere, P. Poizot and J. M. Tarascon, *Nat. Mater.* 2009, **8**, 120.
20. S. Wang, L. Wang, K. Zhang, Z. Zhu, Z. Tao and J. Chen, *Nano Letters* 2013, **13**, 4404.
21. Z. Song, Y. Qian, X. Liu, T. Zhang, Y. Zhu, H. Yu, M. Otani and H. Zhou, *Energy Environ. Sci.* 2014, **7**, 4077.
22. Y. Liang, Z. Tao and J. Chen, *Adv. Energy Mater.* 2012, **2**, 742.
23. P. Sharma, D. Damien, K. Nagarajan, M. M. Shaijumon and M. Hariharan, *J. Phys. Chem. Lett.* 2013, **4**, 3192.
24. X. Han, C. Chang, L. Yuan, T. Sun and J. Sun, *Adv. Mater.* 2007, **19**, 1616.
25. Z. Song, H. Zhan and Y. Zhou, *Chem. Commun.* 2009, 448.
26. B. Genorio, K. Pirnat, R. Cerc-Korosec, R. Dominko and M. Gaberscek, *Angew. Chem., Int. Ed.* 2010, **49**, 7222.
27. Y. Hanyu and I. Honma, *Sci. Rep.* 2012, **2**, 453.
28. T. Nokami, T. Matsuo, Y. Inatomi, N. Hojo, T. Tsukagoshi, H. Yoshizawa, A. Shimizu, H. Kuramoto, K. Komae, H. Tsuyama and J.-i. Yoshida, *J. Am. Chem. Soc.* 2012, **134**, 19694.
29. Y. Park, D.-S. Shin, S. H. Woo, N. S. Choi, K. H. Shin, S. M. Oh, K. T. Lee and S. Y. Hong, *Adv. Mater.* 2012, **24**, 3562.
30. K. Sakaushi, E. Hosono, G. Nickerl, T. Gemming, H. Zhou, S. Kaskel and J. Eckert, *Nat. Commun.* 2013, **4**, 1485.
31. K. Chihara, N. Chujo, A. Kitajou and S. Okada, *Electrochim. Acta* 2013, **110**, 240.
32. S. Wang, L. Wang, Z. Zhu, Z. Hu, Q. Zhao and J. Chen, *Angew. Chem., Int. Ed.* 2014, **53**, 5892.
33. W. Luo, M. Allen, V. Raju and X. Ji, *Adv. Energy Mater.* 2014, **4**, n/a.
34. C. Luo, Y. Zhu, Y. Xu, Y. Liu, T. Gao, J. Wang and C. Wang, *J. Power Sources*. 2014, **250**, 372.
35. L. Chen, W. Li, Y. Wang, C. Wang and Y. Xia, *R. Soc. Chem. Adv.* 2014, **4**, 25369.
36. H. Qin, Z. P. Song, H. Zhan and Y. H. Zhou, *J. Power Sources*. 2014, **249**, 367.
37. M. Andrzejak, G. Mazur and P. Petelenz, *J. Mol. Struct.* 2000, **527**, 91.
38. H.-g. Wang, S. Yuan, D.-l. Ma, X.-l. Huang, F.-l. Meng and X.-b. Zhang, *Adv. Energy Mater.* 2014, **4**, 1301651.
39. A. Abouimrane, W. Weng, H. Eltayeb, Y. Cui, J. Niklas, O. Poluektov and K. Amine, *Energy Environ. Sci.* 2012, **5**, 9632.
40. W. Deng, X. Liang, X. Wu, J. Qian, Y. Cao, X. Ai, J. Feng and H. Yang, *Sci. Rep.* 2013, **3**, 2671.
41. M. Ghosh, K. Mittal, *Polyimides: fundamentals and applications*, Marcel Dekker, New York, 1996.
42. C. De Luca, C. Giomini and L. Rampazzo, *J. Electroanal. Chem.* 1990, **280**, 145.